

This is an Open Access document downloaded from ORCA, Cardiff University's institutional repository:<https://orca.cardiff.ac.uk/id/eprint/134234/>

This is the author's version of a work that was submitted to / accepted for publication.

Citation for final published version:

Chen, Yongping, Gan, Min, Pan, Shunqi , Pan, Haidong, Zhu, Xian and Tao, Zhengjin 2020. Application of auto-regressive (AR) analysis to improve short-term prediction of water levels in the Yangtze estuary. *Journal of Hydrology* 590 , 125386. [10.1016/j.jhydrol.2020.125386](https://doi.org/10.1016/j.jhydrol.2020.125386)

Publishers page: <http://dx.doi.org/10.1016/j.jhydrol.2020.125386>

Please note:

Changes made as a result of publishing processes such as copy-editing, formatting and page numbers may not be reflected in this version. For the definitive version of this publication, please refer to the published source. You are advised to consult the publisher's version if you wish to cite this paper.

This version is being made available in accordance with publisher policies. See <http://orca.cf.ac.uk/policies.html> for usage policies. Copyright and moral rights for publications made available in ORCA are retained by the copyright holders.





15 **Highlights:**

- 16 1. Further identified the predictive error sources of the NS\_TIDE model.  
17 2. Established the temporal correlation of the predictive errors with AR analysis.  
18 3. Applied AR analysis to correct the predictive errors from the NS\_TIDE model.  
19 4. Improved the short-term water level prediction of the Yangtze estuary.

20

21 **Abstract**

22 Due to the complex interaction between the fluvial and tidal dynamics, estuarine tides are less  
23 predictable than ocean tides. Although the non-stationary tidal harmonic analysis (NS\_TIDE)  
24 model can account for the influence of the river discharge, the predictive accuracy of the water  
25 level in the tide-affected estuaries is yet to be improved. The results from recent studies using the  
26 NS\_TIDE model in the lower reach of the Yangtze estuary showed the best root-mean-square-error  
27 (RMSE) between the predicted and measured water levels being in a range of 0.22 ~ 0.26 m. From  
28 the spectral analysis of the predictive errors, it was also found that the inaccurate description of  
29 tides in the sub-tidal frequency band was the main cause. This study is to develop a hybrid model  
30 in combination of the autoregressive (AR) analysis and the NS\_TIDE model in an attempt to  
31 further improve short-term (time scale of days) water level predictions in the tide-affected estuaries.  
32 The results of the application of the hybrid model in the Yangtze estuary show a significant  
33 improvement for water level predictions in the estuary with the RMSE of 24h prediction being  
34 reduced to 0.10 ~ 0.13 m.

35

36 **Keywords:** water level prediction; estuarine tides; Yangtze estuary; NS\_TIDE; Autoregressive  
37 model



## 38 **1. Introduction**

39 In the recent decades, estuaries have been seen the most suitable places for human settlement,  
40 agriculture, transport, and ecosystem services (Savenije, 2015). The activities of engineering  
41 development such as navigation, coastal construction, and flood protection strongly rely on  
42 accurate predictions of water levels in the estuaries, which can be vital for the safety and  
43 sustainability of the economic development in estuarine communities. In the ocean and coastal  
44 waters, water level fluctuations are mainly generated by the astronomic tides and can be predicted  
45 from the classical harmonic analysis (CHA) model such as the T\_TIDE model (Pawlowicz et al.,  
46 2002) with a relatively high accuracy. However, when tides propagate in an estuary, the shallow  
47 water effect becomes significant, not only influencing their properties (amplitudes and phases),  
48 but also generating the shallow water tidal constituents (Gallo and Vinzon, 2005). In addition, the  
49 spatial variation of the estuarine geometry and the temporal change of the river discharge can  
50 further alter tidal properties in estuaries, making the characteristics of the estuarine tides more  
51 complicated. Therefore, applications of the CHA model, which is incapable of taking the influence  
52 of river discharge into account, will yield relatively inaccurate water level predictions in estuaries,  
53 particularly in the upper tidal reach. Jay (1991) developed a theory for river tide propagation in  
54 convergent channels with strong friction, and Kukulka and Jay (2003a, b) further derived the  
55 improved models describing the time-dependent tidal properties (amplitudes and phases) and  
56 tidally-averaged water levels through the nonlinear interaction of river discharge and tides.  
57 Subsequently, based on the works of Kukulka and Jay (2003a, b) and Jay et al. (2011), Matte et al.  
58 (2013) developed a non-stationary tidal harmonic analysis software package, known as NS\_TIDE  
59 model. Matte et al. (2014) used the NS\_TIDE model to analyse the temporal and spatial variation

60 of tidal-fluvial dynamics in the St. Lawrence fluvial estuary. Their results showed that the model  
61 coefficients of the NS\_TIDE model are location specific, but can be interpolated for other locations.  
62 Pan et al. (2018) compared the performance of the NS\_TIDE model with the Empirical Model  
63 Decomposition method and their results revealed that the NS\_TIDE model is less efficient in  
64 representing the sub-tidal water level fluctuations. Gan et al. (2019) explored the applicability of  
65 the NS\_TIDE model to the tides in the Yangtze estuary and markedly improved its accuracy by  
66 including more sub-tidal components in the non-stationary harmonic analysis, but the predictive  
67 accuracy was found to be compromised by the additional degrees of freedom introduced in the  
68 analysis processes.

69 The results of Pan et al. (2018) and Gan et al. (2019) also clearly elucidated that the errors  
70 from the NS\_TIDE model have strong subtidal (low-frequency) variation, with the periods longer  
71 than one or two days, indicating that the predictive errors in a short period of the past (days or  
72 months) may influence its future predictions of the low-frequency tides. In fact, the predictive  
73 errors of the NS\_TIDE model, which are temporally varying, are found to have strong correlation  
74 in the time series, i.e. the future variations can be closely related to the past behaviour.

75 The AR analysis is expected to establish the auto-regressive (cause-and-effect) relationship  
76 between the recent and past values in the same time series, and uses the established correlation to  
77 predict the future possible values, which can be adopted to correct the tide predictions (Carbajal-  
78 Hernández et al., 2012). To account for the dynamic nature of the physical processes in engineering  
79 applications, the AR model is always linked to the Moving-Average (MA) to form the  
80 Autoregressive Moving Average (ARMA) model, which has been widely used in the areas of  
81 hydrology and oceanography. For example, Petaccia et al. (2006) used a non-linear version of the

82 ARMA model to forecast the sea level under high water events at Venice in Italy. Li et al. (2015)  
83 used the AR model to correct the forecast results of river discharge predicted from hydrological  
84 model and presented the potential problems existed in the application of the AR model. Similarly,  
85 Turki et al. (2015) used the ARMA model to forecast the sea level and fill the sea level gaps in  
86 oceans and coastal areas. Moreover, by considering the sea level pressure, Turki et al. (2015)  
87 improved the predictive accuracy of sea level under the surge conditions. More recently, Chen and  
88 Boccelli (2018) applied the seasonal AR model in the forecast of water demands. The ARMA  
89 models were also successfully used for other purposes such as the short-term forecast of ocean  
90 waves (Ge and Kerrigan, 2016), following the works for the spectral estimation of ocean waves  
91 (Mandal et al., 1992) and the forecast of drifting object trajectories in ocean (Minguez et al., 2012).

92 As shown in previous applications for a promising predictive capability, the AR model is  
93 particularly suitable for processes having a strong “memory” of the past events (Li et al., 2015).  
94 Considering the non-stationary nature of the tides in estuaries, it is proposed in this study that the  
95 AR method is to be implemented along with the NS\_TIDE model as a practical tool to improve  
96 the water level predictions in an estuarine environment. Therefore, the objectives of this study are:  
97 1) to analyse the predictive errors from the NS\_TIDE model applied in the Yangtze estuary as an  
98 example to understand and establish their auto-regressive relationship; 2) to develop a practical  
99 NS\_TIDE&AR hybrid model to correct the predictions from the NS\_TIDE model; and 3) to  
100 examine the predictive accuracy of the NS\_TIDE&AR hybrid model with the hourly measured  
101 data at several hydrometric stations along the Yangtze estuary. It should be noted that due to the  
102 regressive nature of the NS\_TIDE model, the hybrid model developed in this study excludes the  
103 applicability from predicting the water levels at storm scales, where the short-term rapidly varying

104 factors such as meteorological influence may play an important role.

105

## 106 2. Model description

### 107 2.1 Nonstationary tidal harmonic analysis (NS\_TIDE) model

108 In the framework of CHA model for astronomical tides, the tidal amplitudes and phases are  
109 assumed to be constant. However, for the tides in estuaries, their properties (amplitudes and phases)  
110 can be strongly affected by the river discharge, and vary with both the upstream river discharge  
111 and downstream tidal range due to the nonlinear interaction between river discharge and tides. To  
112 provide the capability of achieving a better analytic accuracy than CHA model, based on the  
113 T\_TIDE model (Pawlowicz et al., 2002), the NS\_TIDE model takes account for both external  
114 forces (upstream river discharge and ocean tide) and their nonlinear interactions with the following  
115 equations as suggested by Matte et al. (2013, 2014):

$$116 \quad \eta(t) = \eta_0 + \sum_{k=1}^n A_k \cos(\sigma_k t) + B_k \sin(\sigma_k t) \quad (1)$$

117 where  $\eta(t)$  is the water level in estuary;  $n$  is the number of tidal constituents;  $k$  is the index of  
118 tidal constituents;  $\sigma_k$  is the  $k^{\text{th}}$  tidal frequency; and  $t$  is time. In Eq.(1),  $\eta_0$  describes the tidally-  
119 averaged water levels (frequency less than diurnal tides), commonly known as the stage model  
120 part of the NS\_TIDE model and the other terms at the right-hand side represent the water level  
121 fluctuations whose frequency is equal to or higher than diurnal tides, known as the tidal-fluvial  
122 model part, as:

$$123 \quad \eta_0 = c_0 + c_1 Q^{ps}(t - t_Q) + c_2 \frac{R^{qs}(t-t_R)}{Q^{rs}(t-t_Q)} \quad (2)$$

$$124 \quad A_k = d_{0,k}^c + d_{1,k}^c Q^{pf}(t - t_Q) + d_{2,k}^c \frac{R^{qf}(t-t_R)}{Q^{rf}(t-t_Q)} \quad (3)$$

125 
$$B_k = d_{0,k}^s + d_{1,k}^s Q^{p_f}(t - t_Q) + d_{2,k}^s \frac{R^{q_f}(t-t_R)}{Q^{r_f}(t-t_Q)} \quad (4)$$

126 where the subscripts  $s$  &  $f$  denote the stage model and tidal-fluvial model, respectively; ( $p_s$ ,  $q_s$ ,  
 127  $r_s$ ) & ( $p_f$ ,  $q_f$ ,  $r_f$ ) are unknown exponents in the stage and tidal-fluvial models, which can be  
 128 determined by the iterative process using *fmincon* function in MATLAB;  $Q(t)$  is the low-passed  
 129 river discharge at the upstream reference location;  $R(t)$  is the tidal range at the downstream  
 130 reference location which takes the greater diurnal tidal range in the cases of the semi-diurnal tide  
 131 regimes;  $t_Q$  &  $t_R$  are the estimated time lags of the river discharge from the upstream reference  
 132 location and the tide wave from the downstream reference location propagating to a given location  
 133 where water levels are modelled by the NS\_TIDE model, respectively;  $c_i$  &  $d_{i,k}$  ( $i= 0-2$ ) are  
 134 unknown parameters which can be determined by the iteratively reweighted least-square analysis  
 135 approach (Codiga, 2011; Holland and Welsch,1977; Leffler and Jay, 2009). The time-dependent  
 136 amplitude ( $D_k$ ) and phase ( $\alpha_k$ ) of the  $k^{\text{th}}$  tidal constituent are calculated as,

137 
$$D_k = \sqrt{A_k^2 + B_k^2} \quad \text{and} \quad \alpha_k = \tan^{-1} \left( \frac{B_k}{A_k} \right) \quad (5)$$

138 2.2 Auto-regressive (AR) analysis

139 The AR analysis is to establish the temporal correlation between the stochastic events in a  
 140 time series, so to improve the predictions by taking account of the past behaviour of the variable.  
 141 With the AR analysis being described in Torres et al. (2005) and Carbajal-Hernández et al. (2012),  
 142 the temporal relationship of a variable, taking the difference of the water level computed by the  
 143 NS\_TIDE model and the measurements  $\Delta\eta(t)$  as an example in this study, can be expressed as:

144 
$$\Delta\eta(t) = \varepsilon_t + \sum_{i=1}^p \phi_i \Delta\eta(t - i) \quad (6)$$

145 where,  $\varepsilon_t$  is a random disturbance series following the stochastic process of white noise;

146  $\phi_1, \phi_2, \phi_3, \dots, \phi_p$  are the autoregressive coefficients, which can be determined by the least-square  
147 method; and  $p$  is the model order of the autoregressive process.

148 In Eq. (6), the AR analysis order  $p$  should be sufficiently large to fairly represent the stochastic  
149 process, but a larger  $p$  will increase the degree of freedom which may on the other hand increase  
150 the instability of the model. Therefore, a criterion needs to be introduced to determine the optimal  
151 model order. To achieve the right balance of model performance and the order of freedom, in  
152 practice, the Akaike's Information Criterion (AIC) (Shibata, 1976; Torres et al., 2005) has been  
153 commonly used in determining the model order  $p$ , which can be expressed as,

$$154 \quad \text{AIC} = \ln[\hat{\sigma}_a^2(p)] + 2 \frac{(p+1)}{N} \quad (7)$$

155 where  $\hat{\sigma}_a^2(p)$  is the model variance and  $N$  is the number of samples. The model variance  
156 represents the model performance during the fitting period, while the model order reflects the  
157 degree of freedom of the model. With a larger  $p$ , the model variance may become smaller, but  
158 model's degree of freedom would increase. Conversely, when  $p$  is smaller, the model variance may  
159 become larger, but model's degree of freedom will reduce. Lower model's degree of freedom can  
160 make the model more stable and help deal with over-fitting problem. In determining the optimal  
161 combination of model performance and model stability, the smallest AIC number as expressed in  
162 Eq. (7) is to be sought. Smallest AIC number indicates that the AR model has the best balance  
163 between the performance and the degree of freedom of the model.

164 In addition, to use the AR analysis, the time series of the variable should also be ascertained  
165 to be stationary, where the time series of the variable should have no significant upward or  
166 downward variation trends and they have consistent statistical characteristics such as the mean  
167 value or variance. Therefore, the data stationarity test (Kwiatkowski et al., 1992) should be

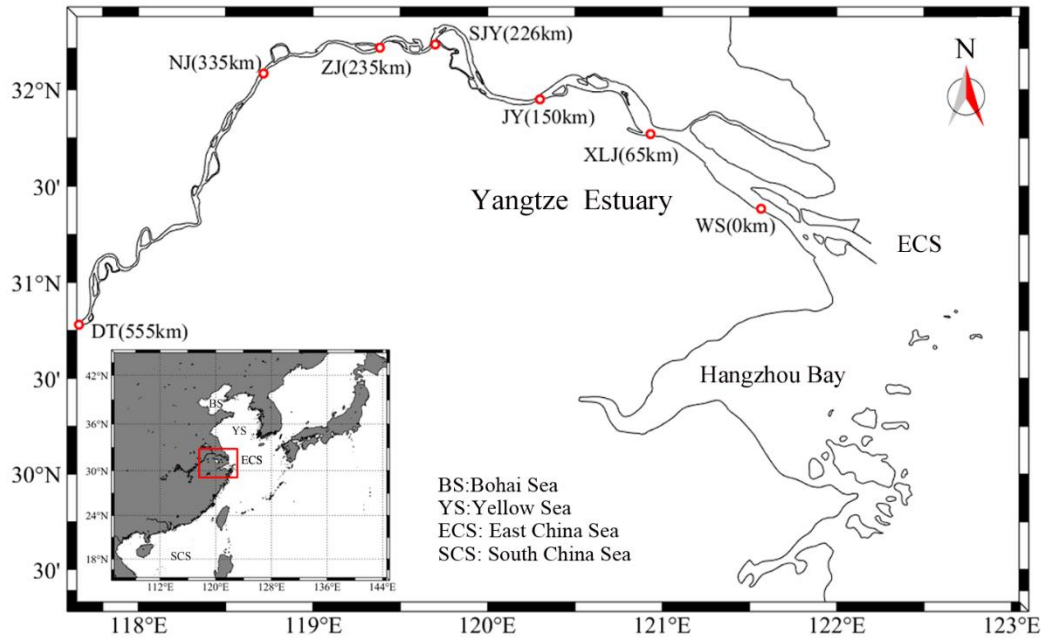
168 conducted prior to the model construction. In this study, the Augmented Dickey-Fuller Unit Root  
169 Test (Cavaliere and Georgiev, 2007) is used to test the stationarity of the temporal variation of the  
170 errors from the NS\_TIDE model. Should the stationarity test fail, the difference method (Peters et  
171 al., 1998) will have to be applied to ensure the stationarity of the data set.

172

### 173 **3. Study site & Field data**

#### 174 3.1 Yangtze estuary

175 Yangtze estuary is located in the middle east coast of China where the Yangtze River meets the  
176 East China Sea (**Fig. 1**). The river discharge into the Yangtze estuary has a significant seasonal  
177 variation pattern. Usually, the flood season is from May to October and the dry season starts from  
178 November and ends in April in the following year (Lu et al., 2015). Based on the recorded data,  
179 the yearly mean river discharge in dry seasons is about 10,000 ~ 20,000 m<sup>3</sup>/s, while in flood  
180 seasons, it is about 45,000 ~ 60,000 m<sup>3</sup>/s (Guo *et al.*, 2016). The tides at the mouth of the Yangtze  
181 estuary are predominately the semi-diurnal tides, with the mean tidal range being approximately  
182 2.65m (Chen *et al.*, 2016).



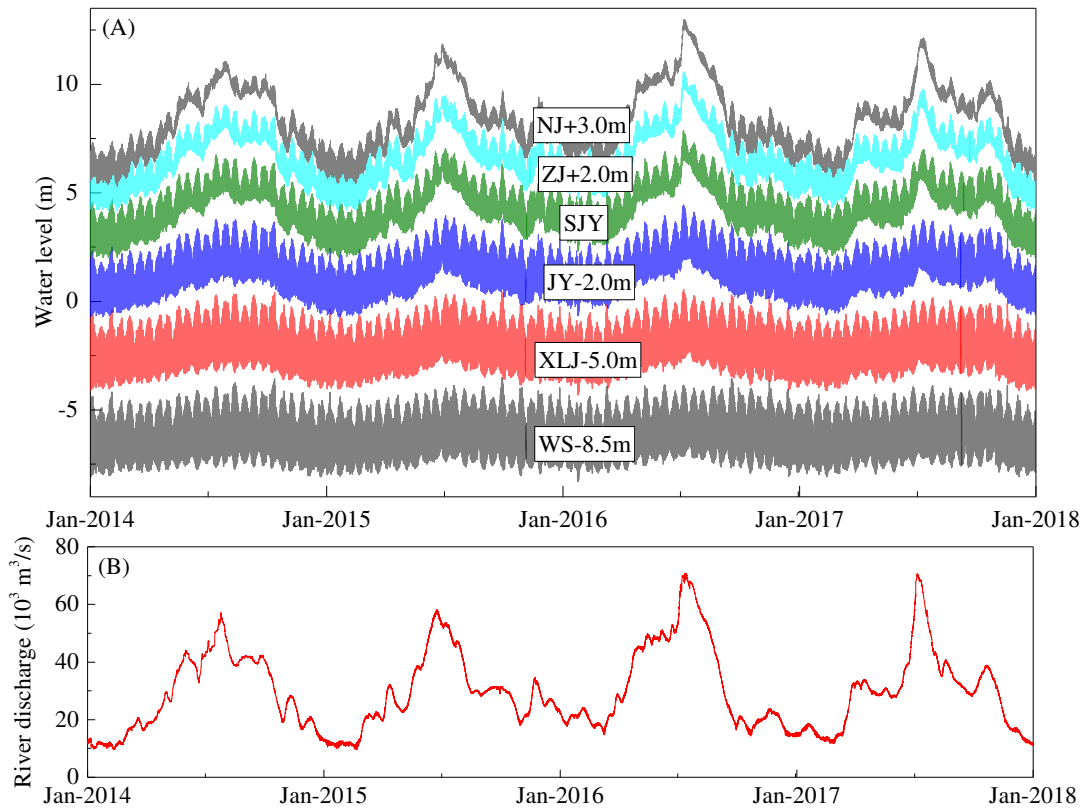
183  
 184 *Fig. 1. Map of the low reach of Yangtze River and locations of hydrometric stations (modified from Gan et*  
 185 *al., 2019)*

### 186 3.2 Field Data

187 Hourly measurements of river discharge at Datong (DT) station and water levels at Nanjing  
 188 (NJ), Zhenjiang (ZJ), Sanjiangying (SJY), Jiangyin (JY), Xuliujing (XLJ), Wusong (WS) stations  
 189 over the period from 2014 to 2017 are available for this study. The longitudinal distance from each  
 190 station to the reference location (WS station), which is the most downstream hydrologic station in  
 191 the estuary, is also illustrated in **Fig. 1**. **Fig. 2** shows the time series of the measured water levels  
 192 at all stations and river discharge at the most upstream station DT. It can be clearly seen that the  
 193 variation of the water levels in the estuary in **Fig. 2(A)** is strongly modulated by the upstream river  
 194 discharge as shown in **Fig. 2(B)**, particularly at the upper reach of the estuary, such as ZJ and NJ  
 195 stations. Except for WS station, where the water levels are least affected by the river discharge,  
 196 the measured water levels at all other stations in the estuary exhibit a strong non-stationarity.  
 197 Therefore, WS station is used as the reference location for ocean tides together with DT station



198 being used as the reference location for river discharge in this study.



199  
200 *Fig. 2. Measured water levels at 6 stations along the Yangtze estuary (A) (see Fig. 1 for their locations);*  
201 *and River discharge measured at DT station (B)*

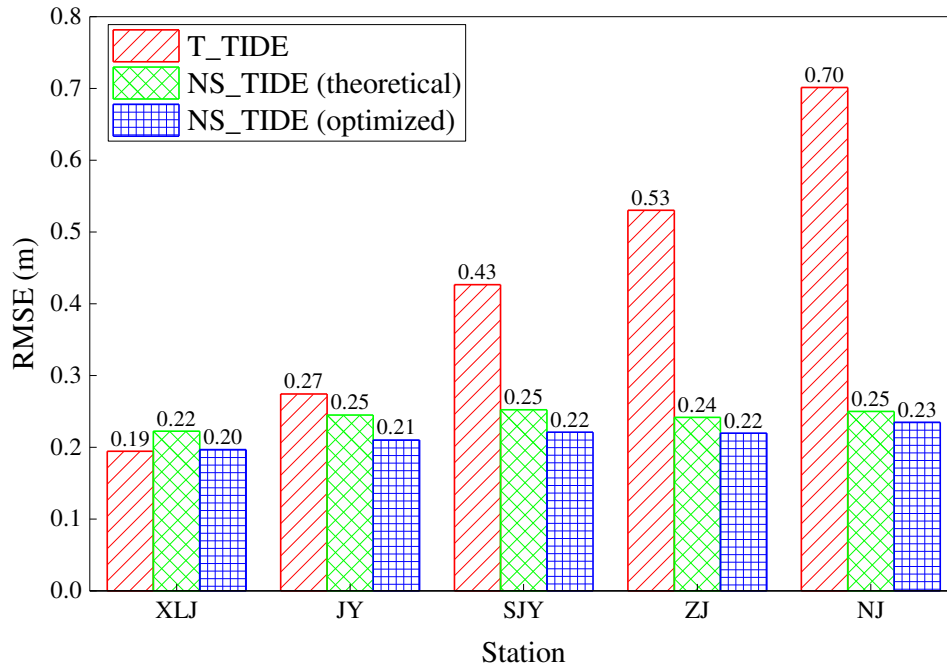
#### 202 4. NS\_TIDE model and Predictive errors

203 To create a framework for inter-comparison and assessment of the improvement of the newly  
204 proposed method, the NS\_TIDE model, which is similar to that used in the work of Gan et al.  
205 (2019), is applied to the study site over the entire 4-year period of the available measurements  
206 (January 2014 - December 2017). Within the measurement period, the measured water levels over  
207 8785 hours (i.e. 8785 hourly measurements) are used to regress the model coefficients of the  
208 NS\_TIDE model. To account for the seasonality of the river discharge and dynamic nature of the  
209 tides, those coefficients are renewed regularly after a certain period of time (D hours), which is  
210 360 hours in this study, in considering the neap-spring tidal cycles.

211 It should be noted that when the regression procedure can be carried out over a sufficiently  
212 long period of the measurements that covers the all (low and high) river flow conditions, updating  
213 the NS\_TIDE model parameters may not be necessary as suggested by Matte et al. (2013).  
214 However, as can be seen from **Fig. 2(B)**, the measurements available to this study only cover a  
215 period of low flow years (2014 - 2015) and a period of high flow years (2016 – 2017), and the  
216 regression procedure can only cover part of the entire measurement period, it therefore becomes  
217 necessary to update the model parameters regularly as aforementioned in this study to better  
218 capture the seasonal variation of the river discharge and improve the model performance. However,  
219 updating the model parameters of the NS\_TIDE model sometimes may also incur discontinuity in  
220 the model parameters, but this was found to be rather minor in the present study.

221 To further illustrate the applicability of the NS\_TIDE model in the Yangtze estuary with the  
222 proposed settings, the results from T\_TIDE, NS\_TIDE with theoretical exponents, and the  
223 NS\_TIDE model with the optimised exponents in this study are compared. As the NS\_TIDE model  
224 is developed on the frameworks of Kukulka and Jay (2003a, b), it is assumed that similar or even  
225 smaller magnitude of the tidal discharge relative to the river discharge, and a moderate estuarine  
226 shape convergence. Although at the downstream reach of Yangtze estuary, the mean tidal prism  
227 can be around 10 times larger than the mean river discharge, which may partly limit the  
228 applicability of the NS\_TIDE model, the iterative method to determine the exponents in Eqs. (2~4)  
229 would be the effective way to relax this requirement in the assumptions. In terms of the geometry  
230 of the estuary, the very low reach of the Yangtze estuary (from estuary mouth to JY) covers about  
231 200 km and the channel width decreases from nearly 20 km to 3 km toward the upstream, while  
232 in the upstream reach of the estuary (JY - DT), it keeps nearly uniform width though with the

233 presence of meanders (Guo et al. 2015). Therefore, it can be reasonably assumed that the variation  
234 of the channel width meets the requirement of the NS\_TIDE model, which was also indicated in  
235 the studies of Zhang et al. (2012) and Cai et al. (2014). The results of Gan et al (2019) also  
236 illustrated the applicability of the NS\_TIDE model in the Yangtze estuary with confidence. For the  
237 NS\_TIDE model with theoretical exponents, the following values as suggested by Kukulka and  
238 Jay (2003a, b) are used: ( $p_s = 2/3$ ,  $q_s = 2$ ,  $r_s = 4/3$ ) & ( $p_f = 1$ ,  $q_f = 2$ ,  $r_f = 1/2$ ). From  
239 the tests carried out during the period between 2014 and 2017, the RMSE values for all 3 models  
240 are compared in **Fig. 3**. The results show that the NS\_TIDE model with the iteratively optimized  
241 exponents as used in this study preforms better than the NS\_TIDE model with the theoretical  
242 exponents and the classical harmonic analysis (T\_TIDE) model (Pawlowicz et al. 2002), with the  
243 RMSE values being in the range of 0.20 – 0.25 m. At XLJ station, which is closest to the estuary  
244 mouth where the effect of the river discharge on the water level is expected to be the least, the  
245 classical harmonic analysis (T\_TIDE) model would perform better. The results further illustrate  
246 the applicability of the NS\_TIDE model in the Yangtze estuary.



247

248

*Fig. 3. Comparison of the RMSE values of the T\_TIDE model and the NS\_TIDE model with theoretical and iteratively optimized exponents.*

249

250

With the applications of the NS\_TIDE model, **Fig. 4** shows the analysed tidal amplitudes and

251

phases at ZJ station from the NS\_TIDE model. As shown in **Fig. 4**, during the period from 2014

252

to 2017, there are 4 flood-dry seasonal variations as indicated by the river discharge measured at

253

DT station. The tide analysis shows a clear modulation of the seasonal river discharge variations

254

on the tidal amplitudes and phases of  $M_2$  and  $S_2$  tidal constituents. The tidal amplitudes of  $M_2$  and

255

$S_2$  tidal constituents decrease with the increase of river discharge, while their phases increase with

256

the increase of river discharge. The variation of the tidal amplitudes and phases of  $M_2$  and  $S_2$  tidal

257

constituents reflects the effect of frictional dissipation and retardation of river discharge on the

258

propagation of tidal waves. In addition, it should be noticed that the variation of the tidal

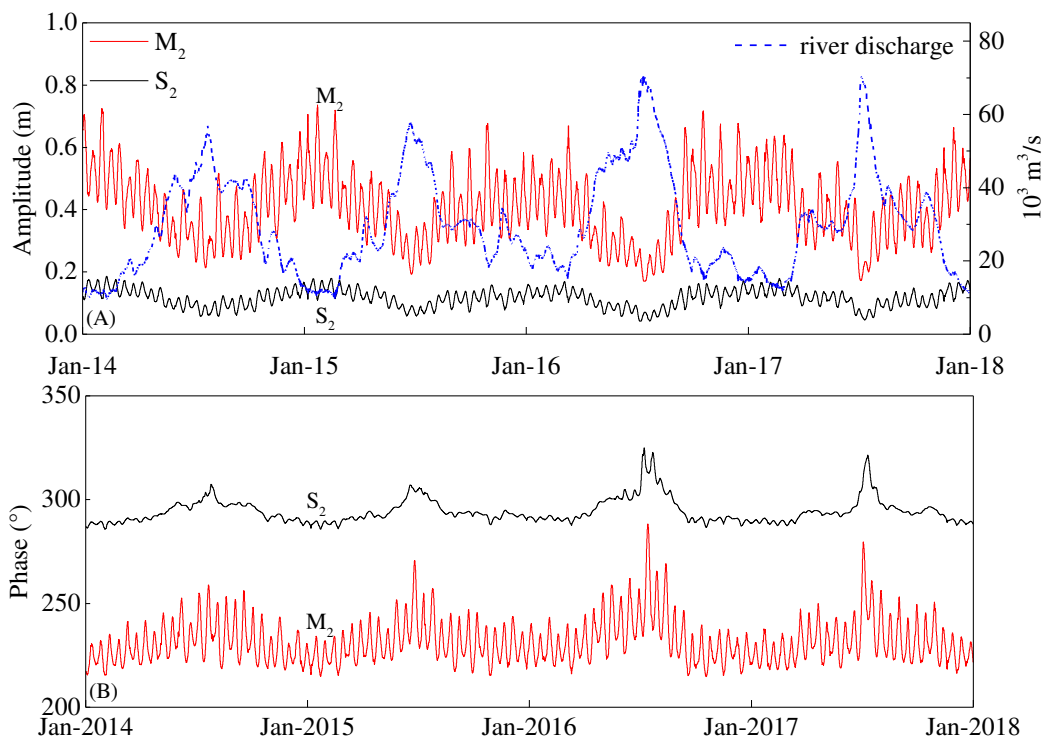
259

amplitudes and phases of  $M_2$  and  $S_2$  tidal constituents presents fortnightly variation patterns. The

260

annual and fortnightly variation cycles of the amplitudes and phases of  $M_2$  and  $S_2$  tidal constituents

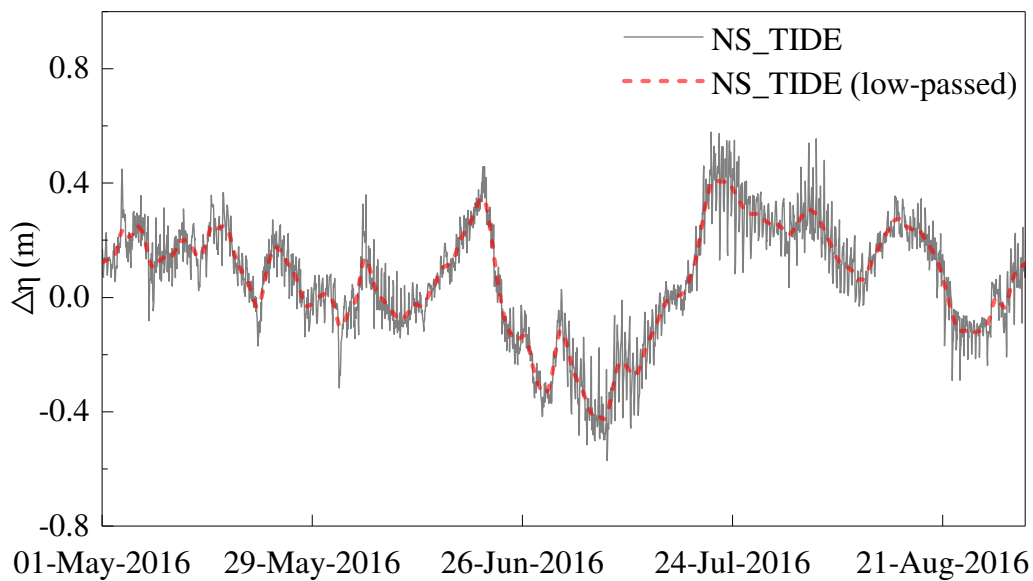
261 correspond to the annually-varied upstream river discharge at the DT station and fortnightly-varied  
 262 (neap-spring cycle) tidal ranges at WS station, which is reflected in the Eq. (1). Comparing the  
 263 decreased tidal amplitudes for  $M_2$  and  $S_2$  during the annual peak river discharges (**Fig. 4**) with the  
 264 increased total water levels at those peaks shown in **Fig. 2**, clearly indicates that the lower  
 265 frequency tidal constituents can make a considerable contribution to the total water level, which is  
 266 a key aspect to be investigated in the following sections.



267  
 268 *Fig. 4. The influence of the river discharge on: (A) tidal amplitudes; and (B) phases of  $M_2$  and  $S_2$  tidal*  
 269 *constituents at ZJ station.*

270 To obtain the predictive errors of the NS\_TIDE model relative to the field measurements, the  
 271 water levels between January 2015 and December 2017 are predicted at 5 stations: XLJ, JY, SJY,  
 272 ZJ and NJ and the root-mean-square-error (RMSE) values of the predicted values relative to the  
 273 measurements are calculated. **Fig. 5** shows the predictive errors of the NS\_TIDE model at ZJ  
 274 station superimposed on their low-passed values. The low-passed filtering process is to filter the

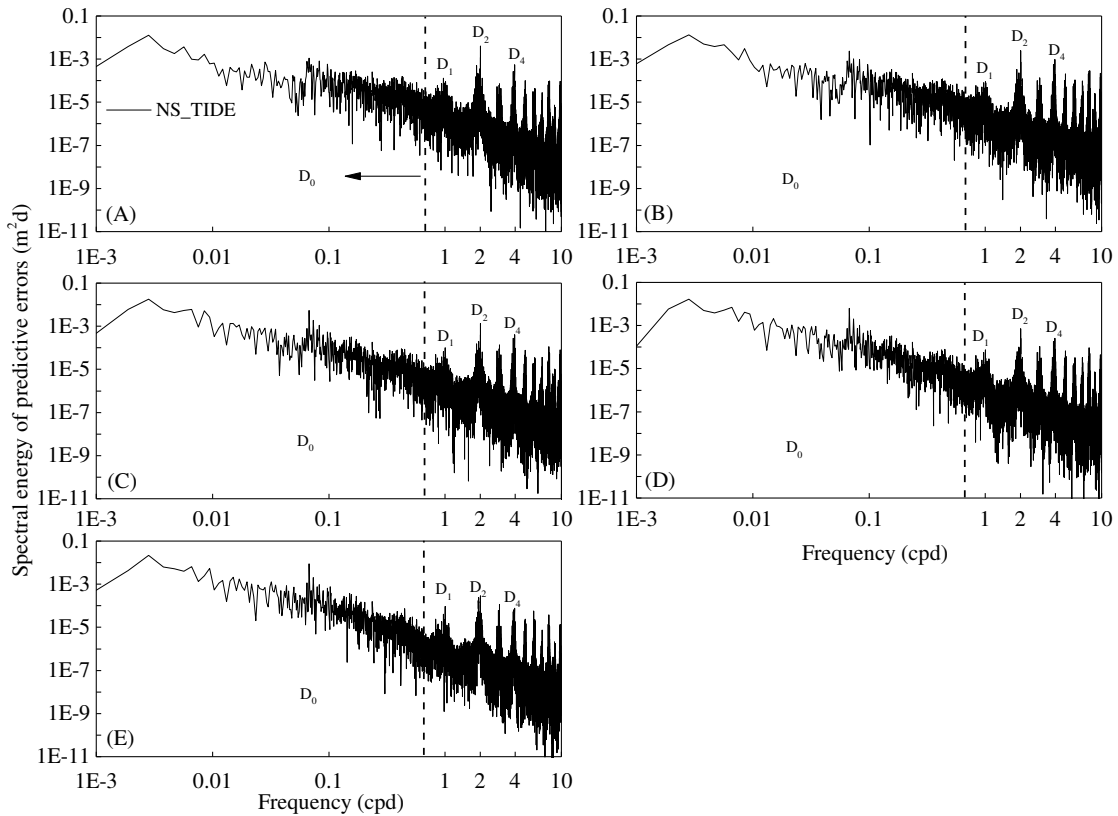
275 fluctuation whose frequency is larger than 1 cycle per day (cpd). The results show that the  
 276 predictive errors are mainly between  $\pm 0.5$  m with the RMSE value being about 0.25 m. However,  
 277 there are considerable low-frequency fluctuations of the predictive errors (**Fig. 5**), which indicates  
 278 the inaccuracy of the NS\_TIDE model in predicting the water levels with longer period than  
 279 diurnal period. In other words, the predictive errors of the NS\_TIDE model have strong variation  
 280 at the subtidal frequency bands.



281  
 282 *Fig. 5. Predictive errors of the NS\_TIDE model and its related low-passed values at ZJ station.*

283 To further show the energy distribution of the predictive errors of the NS\_TIDE model,  
 284 spectral analysis is also applied. **Fig. 6** shows the spectral energy distribution of the predictive  
 285 errors of the NS\_TIDE model at the 5 stations along the Yangtze estuary. In the frequency domain,  
 286 the results show that the predictive errors of the NS\_TIDE model has the peak spectral energy in  
 287 the subtidal ( $D_0$ ) band. In  $D_0$  band, at the frequency around 0.07 cpd (neap-spring cycle), there is  
 288 a general increasing trend with the decrease of frequency. This means the predictive errors of the  
 289 NS\_TIDE model in  $D_0$  band partly come from inaccurately presenting the neap-spring cycles of

290 estuarine tides. This also justifies the need of updating the model coefficients of the NS\_TIDE  
 291 model after each neap-spring cycle ( $D=360$  points) adopted in this study. The spectral peaks are  
 292 also found at diurnal ( $D_1$ ), semi-diurnal ( $D_2$ ), and quarter-diurnal ( $D_4$ ) tides, but relatively smaller  
 293 than the tides in  $D_0$  band. This implies that the NS\_TIDE model preforms relatively worse in  
 294 modelling the tides from subtidal band than the tides in diurnal or higher frequency tidal bands.



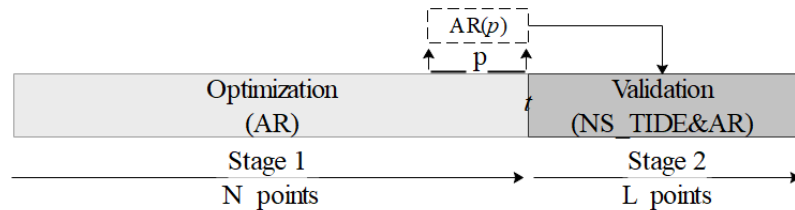
295  
 296 *Fig. 6. Spectral energy distribution of the predictive errors of the NS\_TIDE model at XLJ (A), JY (B), SJY*  
 297 *(C), ZJ (D), and NJ (E) stations.*

298 **5. AR analysis**

299 As shown in **Figs. 5 and 6**, the predictive errors of the NS\_TIDE model is found mainly in  
 300 the subtidal (low-frequency) band. This feature therefore makes the AR analysis more suited to be  
 301 applied. To this end, this study is to introduce the AR analysis through relating the temporal  
 302 correlation of the predictive errors of the NS\_TIDE model to the current or further predictive errors

303 for the NS\_TIDE model by treating the predictive errors as a stochastic process, so that the tide  
 304 predictions from the NS\_TIDE model can be improved, particularly in the low-frequency subtidal  
 305 bands.

306 The AR analysis as illustrated in **Fig. 7** consists of two stages: Stage 1 is to determine the  
 307 parameters required for the AR analysis and optimal model order from the results of the NS\_TIDE  
 308 model and the measurements, and Stage 2 is to apply AR analysis with the NS\_TIDE model (as  
 309 the NS\_TIDE&AR hybrid model) to examine the improvement of the water level predictions.  
 310 Specifically, in Stage 1, a period of  $N$  points (hours) of the results is used to determine the model  
 311 order  $p$  which is optimised by the AIC criterion; and in Stage 2 the constructed AR analysis is used  
 312 to correct the predictions of the NS\_TIDE model over the second part of the data (say  $L$  points),  
 313 which can be regarded as the test period.

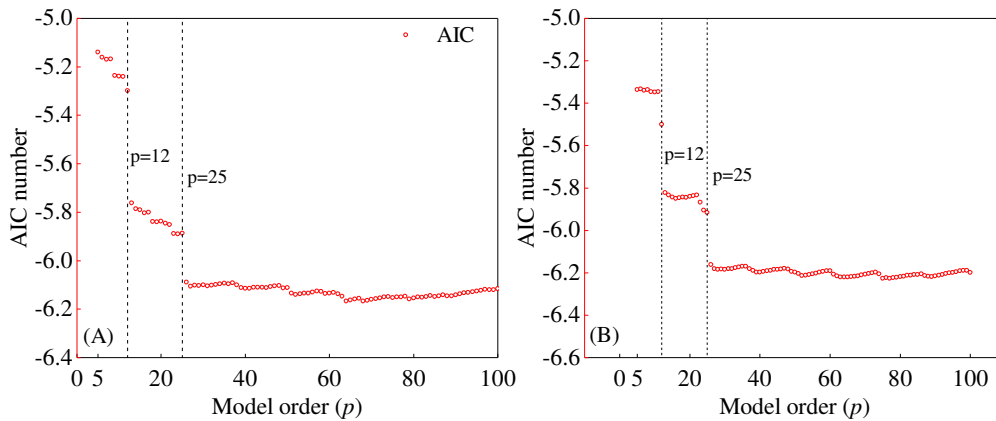


314  
 315 *Fig. 7. Conceptual diagram of the NS\_TIDE&AR hybrid model*

316 For the AR analysis in this study, there are 2 key parameters that should be determined. One  
 317 is the upper limit of the model order  $p$ , and the other is the number of samples  $N$  for the regression  
 318 of the model coefficients. Usually, the model order  $p$  is determined from the partial autocorrelation  
 319 function of time series with constant sample number. However, in this study, the sample is  
 320 considered dynamically changing. Therefore, an upper limit of the model order  $p$  in this study is  
 321 initially specified before the determination of the optimal model order  $p$ . The upper limit of the  
 322 model order  $p$  is determined by preliminary numeric experiments. The determination the upper



323 limit of  $p$  uses 720 hours data points from the NS\_TIDE model, which covers a period of one  
 324 month for 2 spring-neap tide cycles. Model order  $p$  is initially set to 5 and increased to 100. The  
 325 optimal upper limit of  $p$  is then determined when the AIC value reaches a stable value. **Fig. 8**  
 326 shows the variation of the AIC values of AR analysis with different model order  $p$  at XLJ and ZJ  
 327 stations as examples. It can be seen that there are 2 sharp decreases of the AIC values at  $p$  equalling  
 328 to 12 and 25. Those two locations appear to be corresponding to 2 spectral peaks around  $D_2$  and  
 329  $D_1$  in **Fig. 6**. Compared with **Fig. 6**, **Fig. 8** further indicates the 2 spectral peaks may be related to  
 330 both semi-diurnal and diurnal tides whose periods are around 12h and 25h such as  $M_2$  (or  $N_2$ ), and  
 331  $O_1$  tidal constituents. When  $p$  is further increased, the AIC value continues to decrease and reach  
 332 to a stable state at  $p=40$ . However, when  $p$  is larger than 40, the performance of AR analysis is no  
 333 longer significantly improved at both locations. Therefore, in this study, the upper limit of  $p$  at  
 334 each station is set to 40.

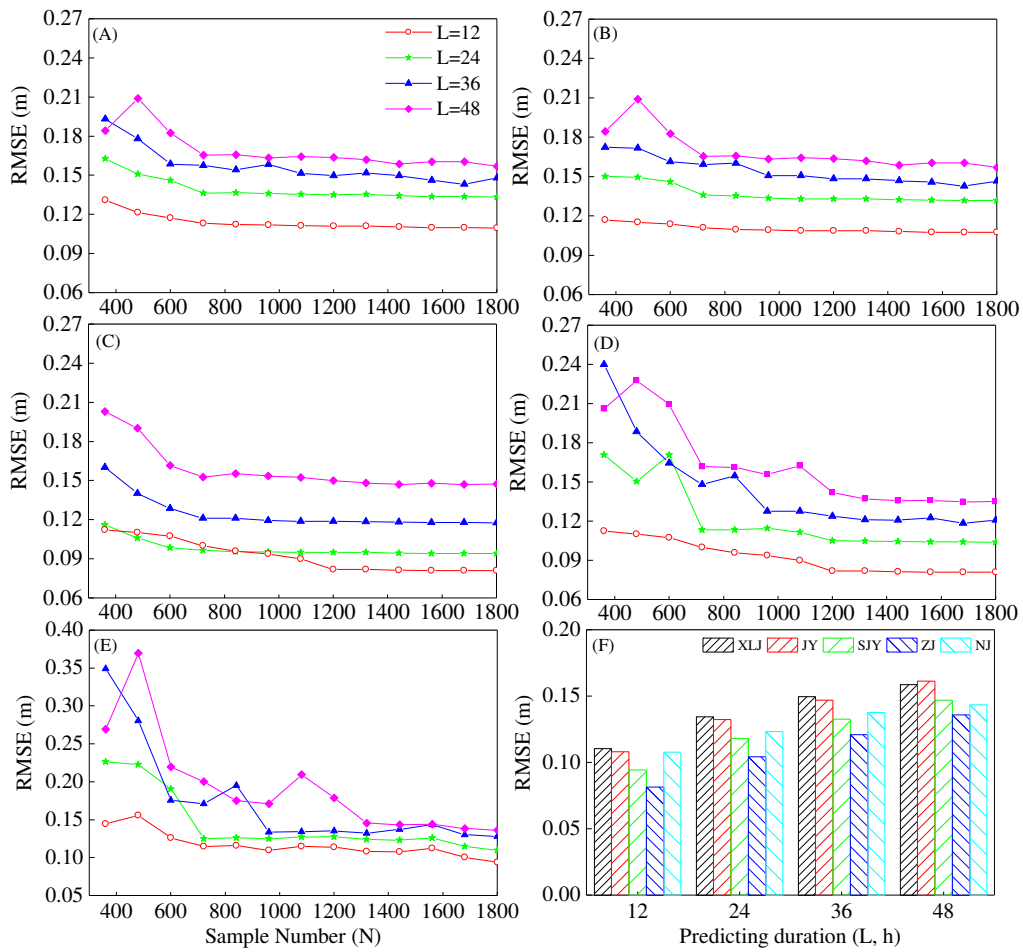


335  
 336 *Fig. 8. Numerical experiment for determining the optimal upper limit of the model order  $p$  at: XLJ (A);*  
 337 *and ZJ (B)*

338 Once the upper limit of the model order  $p$  is determined, the optimum number of samples ( $N$ )  
 339 is another key parameter in the AR analysis to calculate the autoregressive coefficients. For the

340 steady cases,  $N$  can be regarded as constant following the works of Torres (2005) and Mirzavand  
341 and Ghazavi (2015). However, for gradually unsteady processes, such as the water levels in this  
342 study, the model's number of samples should be considered as dynamic and requires to be renewed  
343 periodically. In this study, tests are carried out with the hybrid NS\_TIDE&AR model with varying  
344 number of samples ( $N=360-1800$ ) over different predictive durations ( $L=12-48$  hours). **Fig. 9(A-**  
345 **E)** shows the RMSE values of the predictions of the water levels from the hybrid NS\_TIDE&AR  
346 model against the measurements for those tests. Overall, the RMSE values show a decreasing trend  
347 with the increase of  $N$  and the results become stable in almost all cases when  $N$  is greater than  
348 1200 (hours). However, with a large  $N$ , the computational costs will also become higher and  
349 fluctuations of the RMSE values may occur at some stations due to the over-fitting. To balance the  
350 model accuracy and computational costs, the number of samples of the NS\_TIDE&AR model at  
351 all stations are set to 1440 (corresponding to 1440 hours), which is equivalent to a 2-month period.  
352 **Fig. 9(F)** shows the comparison of RMSE values when  $N=1440$  for different predictive durations,  
353 illustrating a high consistency and a slight increasing trend when the predictive duration increases  
354 from 12 to 48 hours, but all within a range of 0.08 to 0.16 m.

355



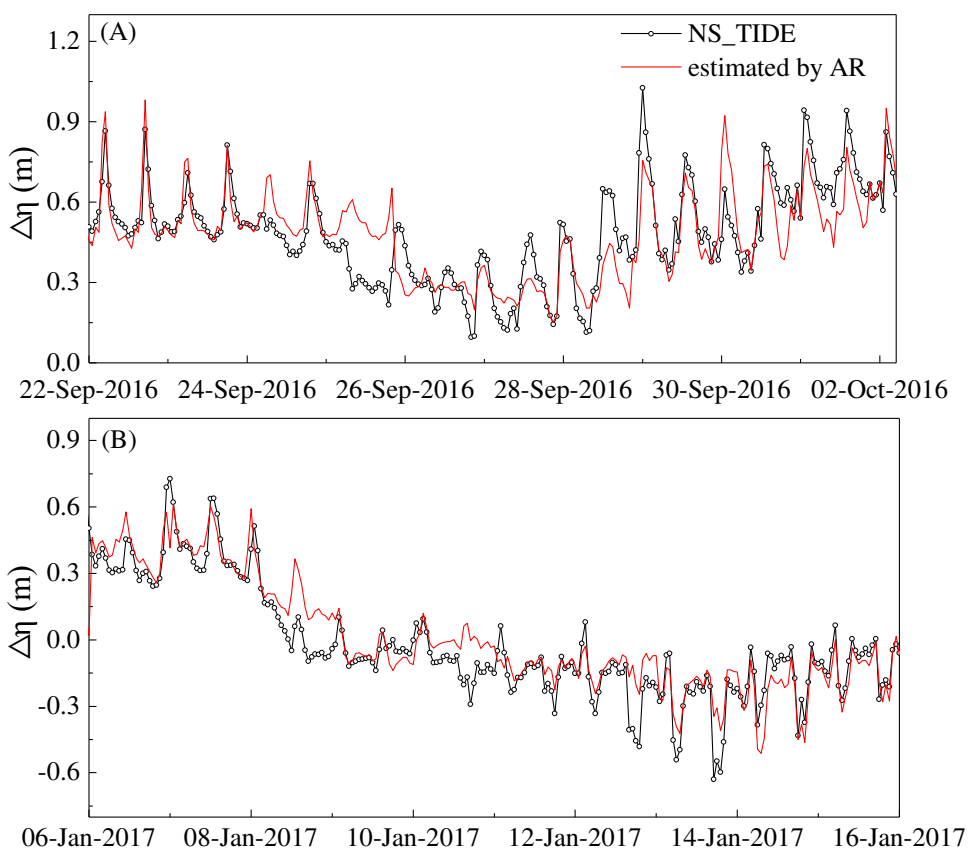
356  
 357 *Fig. 9. Variation of the RSME values of the NS\_TIDE&AR model with the number of samples (N) at: XLJ*  
 358 *(A), JY (B), SJY (C), ZJ (D) and NJ (E) stations; and the comparison of the RMSE values when*  
 359 *N=1440(F), for different predicting durations.*

360 When the predictive errors of the NS\_TIDE model are dynamically modelled by the AR  
 361 model, the non-stationarity tests are conducted on the samples prior to constructing the AR model.  
 362 It is found from the tests that the field data at this study mostly conforms the required stationarity.  
 363 However, while larger temporal variations are discovered in the measurement data, the temporal  
 364 gradients of the predictive errors are calculated and used in the AR analysis, and then an additional  
 365 inverse transformation is used.

366 Following the construction of the AR model in Stage 1, it can now be applied as illustrated in  
 367 **Fig. 7** (Stage 2). Taking the predictive errors of the NS\_TIDE model in September 2016 (flood

368 season) and January 2017 (dry season) at ZJ station as examples, **Fig. 10** shows the comparisons  
 369 of the predictive errors from the NS\_TIDE model and those estimated by the AR model. It can be  
 370 clearly seen that the errors estimated by the AR analysis agree well with those from the NS\_TIDE  
 371 model. The errors in general are modulated by the tides and are larger during the flooding phase  
 372 and lower during the ebbing phase. The envelope curve of the predictive errors of the NS\_TIDE  
 373 model in **Fig. 10** indicates the seasonal pattern for the predictive errors, which reflects its longer  
 374 period variations. This can also be seen as the spectral peak at  $D_0$  band in **Fig. 6**. The results clearly  
 375 illustrate that the AR analysis is capable of estimating the predictive errors from the NS\_TIDE  
 376 model once it is calibrated and trained up a high level of accuracy, which provides an effective  
 377 remedy for the NS\_TIDE model in increasing its accuracy in water level predictions.

378

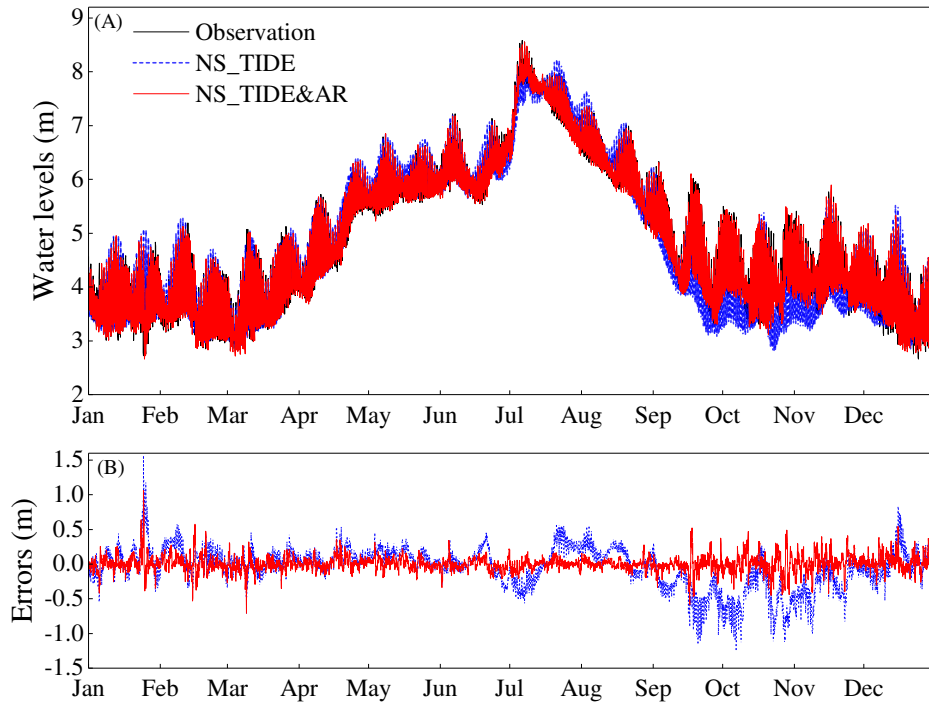


379

380 *Fig. 10. Comparison of the predictive errors from the NS\_TIDE model and those estimated by the AR*  
381 *analysis over flood (A) and dry (B) seasons at ZJ station*

382 To examine the overall performance, the hybrid NS\_TIDE&AR model is applied to the study  
383 site over the entire period between March 2015 and December 2017, where the measurements are  
384 available. For the 24-h ( $L=24$ ) prediction, **Fig. 11(A)** compares the predicted water levels from  
385 both the NS\_TIDE and the hybrid NS\_TIDE&AR models with the observed water levels in 2016  
386 at ZJ station and **Fig. 11(B)** shows the corresponding difference for the sake of clarity. The  
387 predicted water levels at ZJ station from both models agree well with the measurements in general,  
388 but their differences shown in **Fig. 11(B)** clearly indicate that the hybrid NS\_TIDE&AR model  
389 outperforms the NS\_TIDE model with a significant improvement. The predictive errors associated  
390 with the seasonal variation pattern from the NS\_TIDE model are largely eliminated by the hybrid  
391 model, and therefore overall accuracy of the predictions is significantly improved.

392

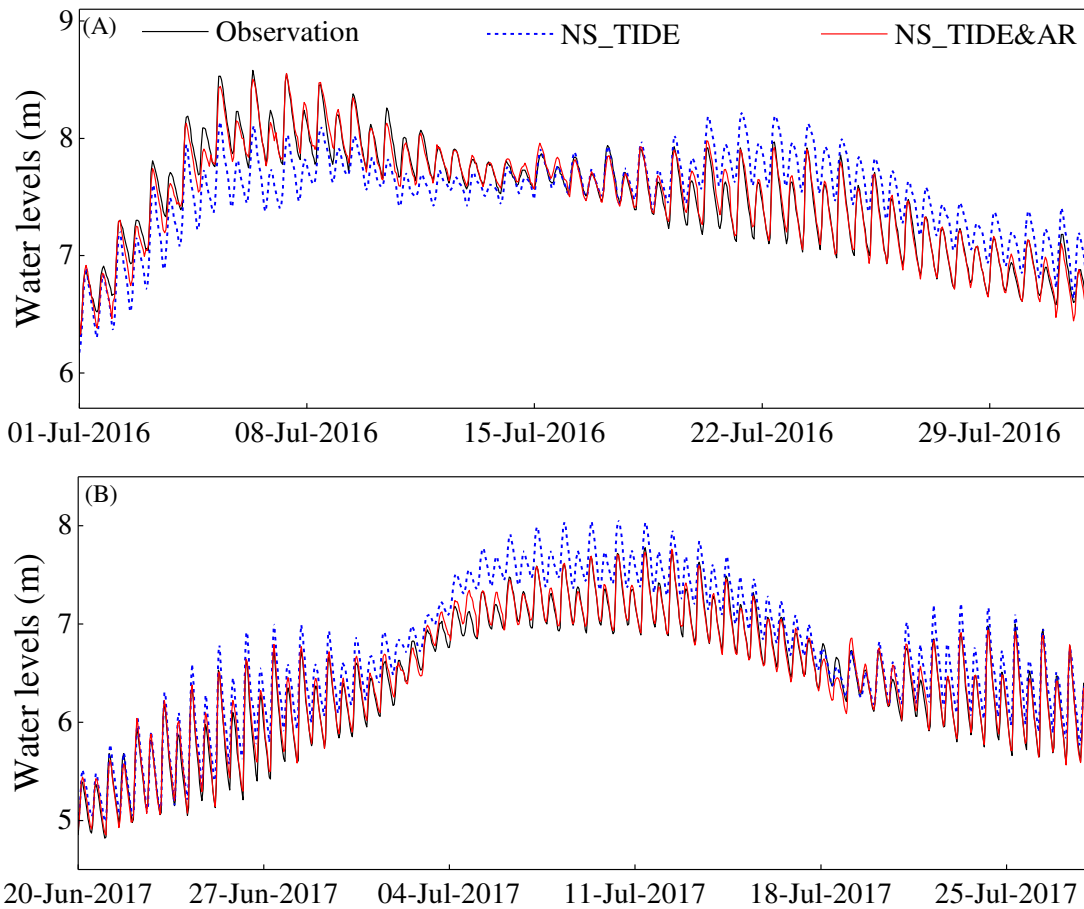


393

394 *Fig. 11. Comparison of all the observed water levels in 2016 and the water levels predicted by the*

395 *NS\_TIDE and NS\_TIDE&AR models (A) and their predictive errors (B) at ZJ station.*

396 For the purpose of flood protection, water level prediction during the flood seasons is  
 397 particularly important. Therefore, **Fig. 12** further shows the comparison of the predicted water  
 398 levels by the NS\_TIDE and NS\_TIDE&AR models with the measurements at ZJ station during  
 399 two flood seasons in 2016 and 2017. The predicted water levels from the NS\_TIDE&AR model  
 400 are found to match much better with the measurements than those from the NS\_TIDE model in  
 401 flood seasons, where the over- and under- predictions of the water level from the NS\_TIDE model  
 402 are largely corrected.

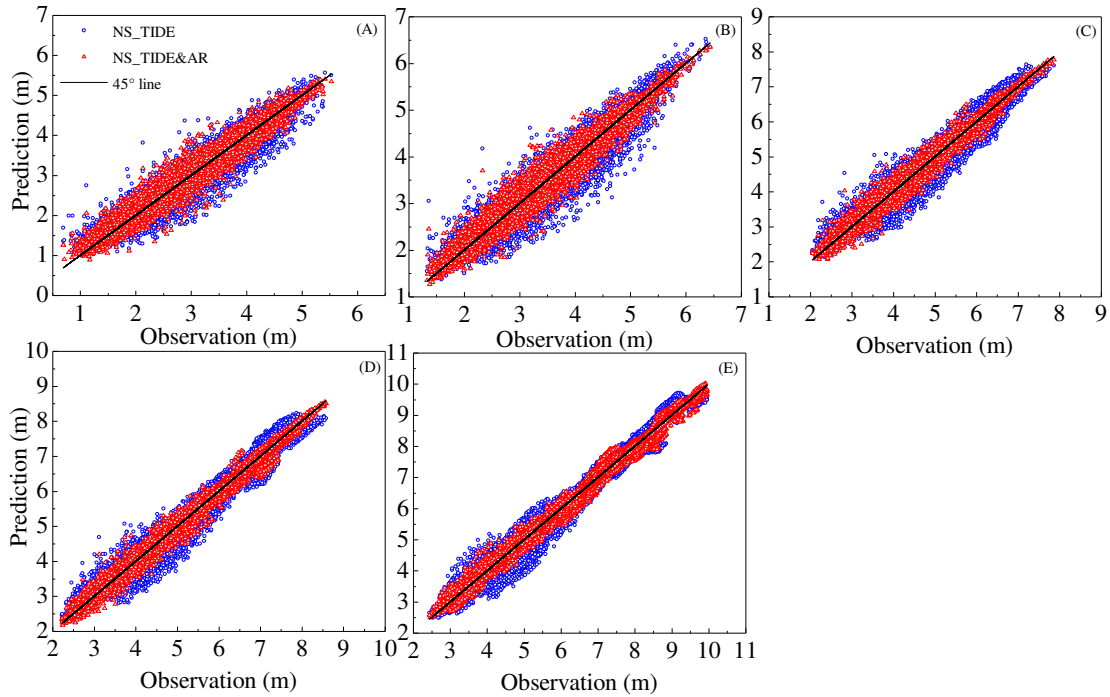


403

404 *Fig. 12. Comparison of the water levels predicted by the NS\_TIDE and NS\_TIDE&AR models with the*  
 405 *measurements at ZJ station during flood seasons of 2016 (A) and 2017 (B).*

406 **Fig. 13** shows the scatter plots of the predicted water levels from both the NS\_TIDE and  
 407 NS\_TIDE&AR models against the measurements at all stations: XLJ, JY, SJY, ZJ and NJ for the  
 408 24-h prediction duration. The results clearly show that the predicted water levels from the  
 409 NS\_TIDE&AR model agree better with the measurements than those from the NS\_TIDE model  
 410 at all stations. At NJ and ZJ stations, the improvement of the NS\_TIDE&AR model over the  
 411 NS\_TIDE model is similar for all waters, but at SJY, JY and XLJ stations, the improvement is seen  
 412 progressively less significant particularly at the mean water level, as the tide forcing strengthens  
 413 towards the estuary mouth as expected. Although, there are occasional outliers from the hybrid

414 model from the perfect fit (45° line), the overall performance of predicting the water levels by the  
 415 NS\_TIDE&AR model at all 5 stations, nevertheless, is significantly improved in comparison with  
 416 the NS\_TIDE model.



417  
 418 *Fig. 13. Scatter plots of the water levels predicted by the NS\_TIDE and NS\_TIDE&AR models with the*  
 419 *measurements at: XLJ (A), JY (B), SJY (C), ZJ (D) and NJ (E) stations.*

## 420 6. DISCUSSION

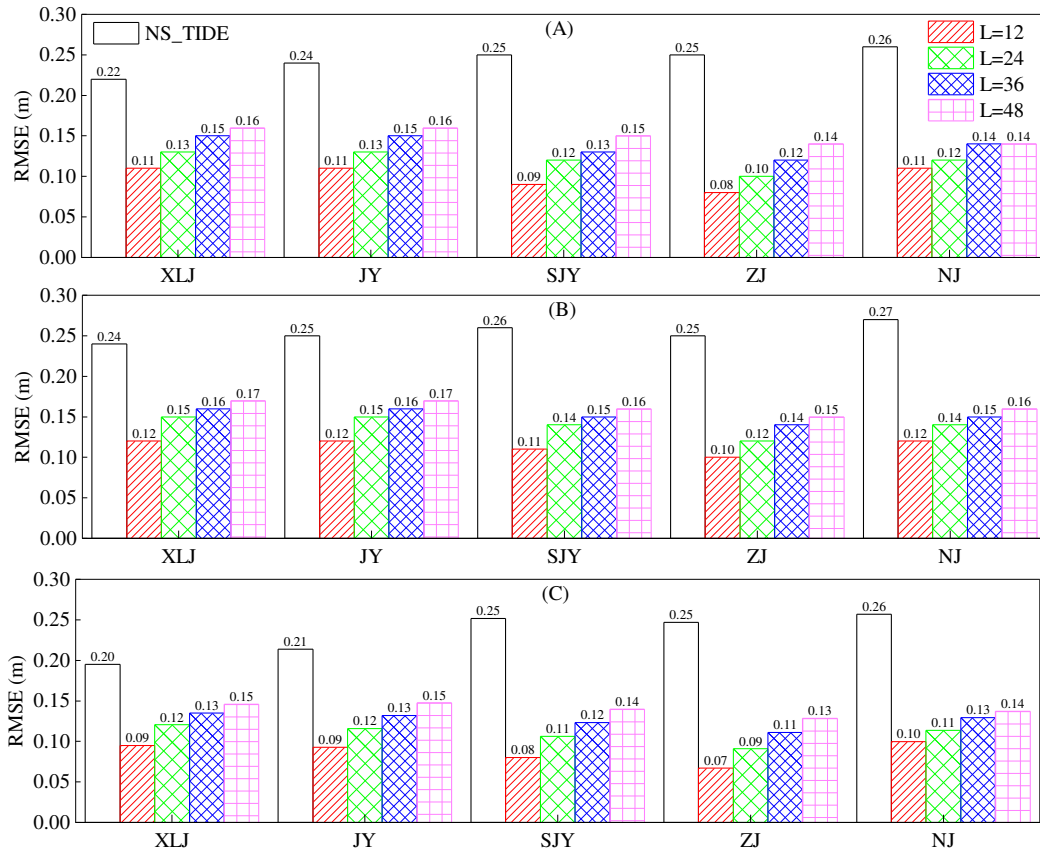
421 To further understand the performance of the hybrid NS\_TIDE&AR model, the hourly water  
 422 levels are predicted by the hybrid model at all stations over a range of short-term prediction  
 423 durations, namely 12, 24, 36 and 48 hours ahead. **Fig. 14(A)** compares the RMSE values of the  
 424 predicted water levels from the hybrid NS\_TIDE&AR and NS\_TIDE models against the  
 425 measurements respectively. Since the RMSE values of the predicted water levels by the NS\_TIDE  
 426 model for durations of 12, 24, 36, and 48 hours are almost the same, therefore, only one value is  
 427 presented at each station in the figure. The results clearly show that the hybrid model significantly



428 reduced the RMSE values in call cases. Taking the 24-hour prediction as an example, the hybrid  
429 model significantly reduces the RMSE values of the NS\_TIDE model from 0.22 ~ 0.26 m to 0.10  
430 ~ 0.13 m. Even for the 48-hour prediction, the longest in the tests, the RMSE values from the  
431 hybrid model are all less than 0.16 m.

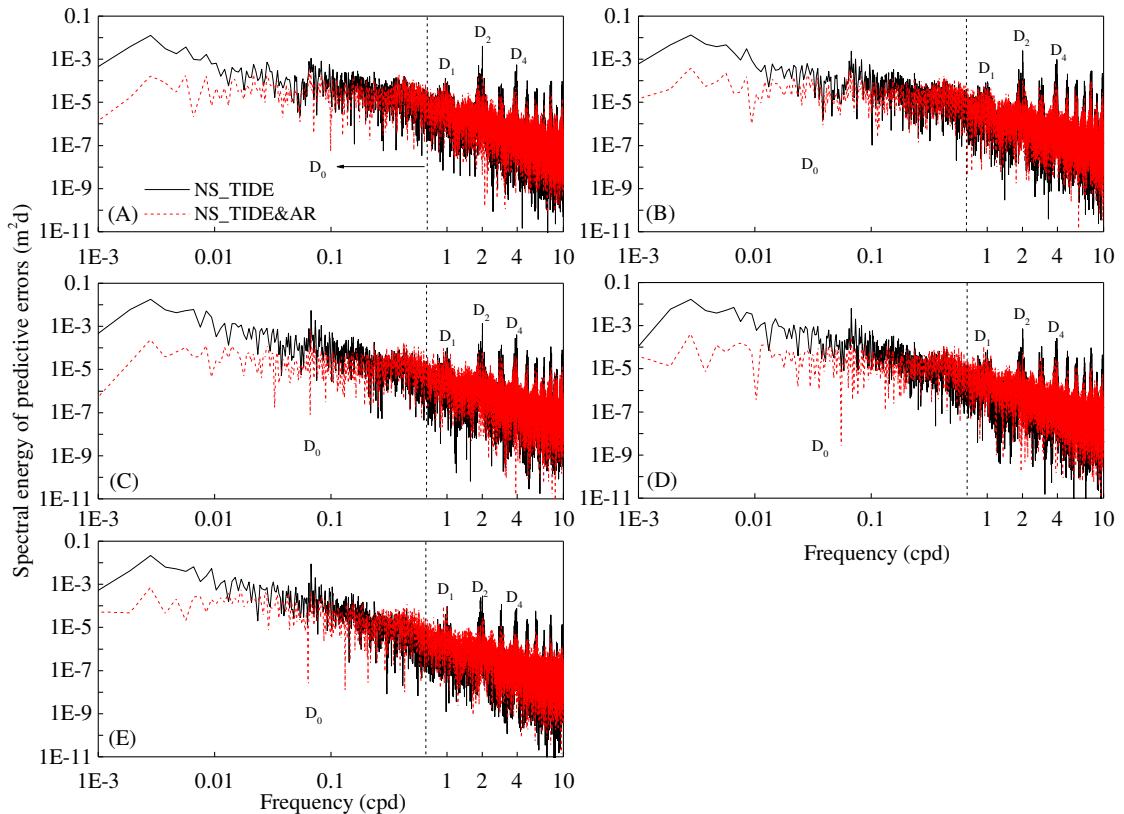
432 **Fig. 14(B)** shows the RMSE values for the high tides, which are important when considering  
433 the flood protection in the estuary. The performance of the hybrid model is also much improved in  
434 comparison with the NS\_TIDE model, although the overall RMSE values are slightly higher than  
435 those shown in **Fig. 14(A)**, but all within 0.02 m. For navigation, where accurate low water level  
436 predictions are as important as the high water levels, the RMSE values of the low water level  
437 predictions are presented in **Fig. 14(C)**. The predictive accuracy of the low water level prediction  
438 of the NS\_TIDE&AR model is even better than that for the high water levels shown in **Fig. 14(B)**.  
439 In summary, the NS\_TIDE&AR model significantly improves the predictive accuracy of the  
440 NS\_TIDE model for both hourly water levels, high water levels, and low water levels.

441



442  
 443 *Fig. 14. RMSE values of the predicted water levels by the NS\_TIDE and NS\_TIDE&AR models over*  
 444 *durations (L) of 12, 24, 36 and 48 hours for: all water levels (A); high water levels (B); and low water*  
 445 *levels (C)*

446 Spectral analysis is also conducted on the time series of the predictive difference of the hybrid  
 447 model to the measurements in the frequency domain. **Fig. 15** shows the spectral energy density of  
 448 the predictive errors of the hybrid NS\_TIDE&AR model at all 5 stations in comparison with that  
 449 of the NS\_TIDE model as shown in **Fig. 6**. It can be seen that the peaks of the spectral energy  
 450 density of the NS\_TIDE&AR model are now much smaller in the  $D_0$  frequency band than that of  
 451 the NS\_TIDE model, which means the NS\_TIDE&AR model achieves a significant improvement  
 452 over the NS\_TIDE model in predicting the water level in the subtidal  $D_0$  band. In the  $D_1$ ,  $D_2$  and  
 453  $D_4$  tidal bands, the spectral peaks of the NS\_TIDE&AR model are also found to be relatively  
 454 smaller than those from the NS\_TIDE model.



456

457 *Fig. 15. Spectral energy distribution of the predictive errors of the NS\_TIDE&AR and NS\_TIDE models*

458

*at: XLJ (A), JY (B), SJY (C), ZJ (D) and NJ (E) stations.*459 **7. CONCLUSIONS**

460

461

462

463

464

465

466

467

In this study, the auto-regressive (AR) analysis is developed and implemented with the existing NS\_TIDE model for predicting the short-term water levels in the Yangtze estuary. The results show that by treating the predictive errors of the NS\_TIDE model as a stochastic process, the AR analysis is capable of correlating robustly the predictive errors over short time periods (~48 hours), which can be used to effectively correct the predictions of water levels from the NS\_TIDE model or possibly any other tide-prediction models. For the 24-h prediction, the RMSE values of the predicted water levels are less than 0.13 m, in comparison with those of 0.22 ~ 0.26 m of the NS\_TIDE model without implementing the AR analysis. Spectral analysis indicates that the main

468 improvement of the NS\_TIDE&AR model over the NS\_TIDE model is in describing the subtidal  
469 tides. Therefore, using AR analysis to estimate the predictive errors of the NS\_TIDE model can  
470 significantly improve the short-term predictions of the water levels in estuary under the influence  
471 of strong river discharge, such as those in the Yangtze estuary.

472

### 473 **CRedit authorship contribution statement**

474 **Yongping Chen:** Conceptualization, Methodology, Writing - Original Draft, Writing - Review &  
475 Editing, Funding acquisition, Supervision. **Min Gan:** Conceptualization, Methodology, Software,  
476 Writing - Original Draft, Writing - Review & Editing, Validation, Formal analysis, Investigation,  
477 Funding acquisition. **Shunqi Pan:** Conceptualization, Methodology, Writing - Original Draft,  
478 Writing - Review & Editing, Funding acquisition, Supervision. **Haidong Pan:** Resources,  
479 Investigation. **Xian Zhu:** Data Curation, Investigation. **Zhengjin Tao:** Data Curation,  
480 Visualization.

481

### 482 **Declaration of interests**

483 The authors declare that they have no known competing financial interests or personal  
484 relationships that could have appeared to influence the work reported in this paper.

485

### 486 **Acknowledgements**

487 This work was partly supported by the National Key R&D Program of China [Grant No:  
488 2017YFC0405401], the Fundamental Research Funds for the Central Universities of China [Grant  
489 Nos: 2017B20214 and 2018B635X14] and the Postgraduate Research & Practice Innovation

490 Program of Jiangsu Province [Grant No: KYCX18\_0602]. The second author also would like to  
491 acknowledge the financial support from the China Scholarship Council (CSC) under PhD  
492 exchange program [201906710022] with Cardiff University. The authors would also like to thank  
493 Pascal Matte for providing the NS\_TIDE model software package.

494

## 495 **References**

496 Cai, H., Savenije, H. H. G., & Toffolon, M. (2014). Linking the river to the estuary: influence of  
497 river discharge on tidal damping. *Hydrol. Earth Syst. Sci.*, 18, 287-304, doi: 10.5194/hess-  
498 18-287-2014.

499 Carbajal-Hernández, J.J., Sánchez-Fernández, L.P., Carrasco-Ochoa, J.A. & Martínez-Trinidad,  
500 J.F. (2012). Assessment and prediction of air quality using fuzzy logic and autoregressive  
501 models. *Atmospheric Environment*, 60, 37-50, doi:10.1016/j.atmosenv.2012.06.004.

502 Cavaliere, G. & Georgiev, I. (2007). Testing for Unit Roots in Autoregressions with Multiple  
503 Level Shifts. *Econometric Theory*, 23, 1162-1215, doi: 10.1017/S0266466607070466

504 Chen, J.C. & Boccelli, D.L. (2018). Forecasting hourly water demands with seasonal  
505 autoregressive models for real-time application. *Water Resources Research*, 54, 879–894,  
506 doi: 2017WR022007.

507 Chen, W., Chen, K., Kuang, C.P., Zhu, D.Z., He, L.L., Mao, X.D., Liang, H.D., & Song, H.L.  
508 (2016). Influence of sea level rise on saline water intrusion in the Yangtze River Estuary,  
509 China. *Applied Ocean Research*, 54, 12-25, doi:10.1016/j.apor.2015.11.002.

510 Codiga, D.L. (2011). Unified tidal analysis and prediction using the UTide Matlab functions,  
511 Technical Report 2011-01. Graduate School of Oceanography, University of Rhode Island,  
512 Narragansett, RI. 59pp. [Available online at

- 513 <ftp://www.po.gso.uri.edu/pub/downloads/codiga/pubs/2011Codiga-UTide-Report.pdf>]
- 514 Gallo, M.N. & Vinzon, S.B. (2005). Generation of overtides and compound tides in Amazon  
515 estuary. *Ocean Dynamics*, 55, 441-448, 10.1007/s10236-005-0003-8.
- 516 Gan, M., Chen, Y., Pan, S., Li, J., & Zhou, Z. (2019). A modified nonstationary tidal harmonic  
517 analysis model for the Yangtze estuarine tides. *J. Atmos. Ocean. Technol.*, 36, 513-525,  
518 doi:10.1175/JTECH-D-18-0199.1.
- 519 Ge, M. & Kerrigan, E.C. (2016). Short-term Ocean Wave Forecasting Using an Autoregressive  
520 Moving Average Model. *11th International Conference on Control (CONTROL)*, Belfast,  
521 UK, doi: 10.1109/CONTROL.2016.7737594.
- 522 Guo, L.C., Wegen, M.V. D., Jay, D.A., Matte, P., Wang, Z.B., Roelvink, D., & He, Q. (2015).  
523 River-tide dynamics: Exploration of nonstationary and nonlinear tidal behavior in the  
524 Yangtze River estuary. *J. Geophys. Res. Oceans*, 120, 3499-3521, 10.1002/2014JC010491.
- 525 Guo, L.C., Wegen, M.V. D., Wang, Z.B., Roelvink, D., & He, Q. (2016). Exploring the impacts  
526 of multiple tidal constituents and varying river flow on long-term, large-scale estuarine  
527 morphodynamics by means of a 1-D model. *J. Geophys. Res. Oceans*, 121(5):1000-1022,  
528 10.1002/2016JF003821.
- 529 Holland, P. W. & Welsch, R.E. (1977). Robust regression using iteratively reweighted least-  
530 squares. *Communications in Statistics-Theory and Methods*, 6(9), 813-827,  
531 doi:10.1080/03610927708827533.
- 532 Jay, D. A. (1991). Green's law revisited: Tidal long-wave propagation in channels with strong  
533 topography. *J. Geophys. Res.*, 96(C11), 20 585–20 598, doi: 10.1029/91JC01633.
- 534 Jay, D. A., Leffler, K., & Degens, S. (2011). Long-Term Evolution of Columbia River Tides. *J.*

535 *Waterw. Port Coastal Ocean Eng.*, 137, 182-191, doi:10.1061/(ASCE)WW1943-  
536 5460.0000082.

537 Kukulka, T. & Jay, D.A. (2003a). Impacts of Columbia River discharge on salmonid habitat: 1. A  
538 nonstationary fluvial tide model. *J. Geophys. Res. Ocean*, 108, 3293,  
539 doi:10.1029/2002JC001382.

540 Kukulka, T. & Jay, D. A. (2003b). Impacts of Columbia River discharge on salmonid habitat: 2.  
541 Changes in shallow-water habitat. *J. Geophys. Res. Ocean.*, 108, 3294, doi:  
542 10.1029/2003JC001829

543 Kwiatkowski, D., Phillips, P.C.B., Schmidt, P., & Shin, Y. (1992). Testing the null hypothesis of  
544 stationarity against the alternative of a unit root. How Sure Are We That Economic Time  
545 Series Have Unit Root? *Journal of Econometrics*, 54, 159-178, doi: 10.1016/0304-  
546 4076(92)90104-Y.

547 Leffler, K.E. & Jay, D. A. (2009). Enhancing tidal harmonic analysis: Robust (hybrid L1/L2)  
548 solutions. *Cont. Shelf Res.*, 29, 78-88, doi:10.1016/j.csr.2008.04.011.

549 Li, M., Wang, J.Q., Bennett, J.C., & Robertson, D. E. (2015). A strategy to overcome adverse  
550 effects of autoregressive updating of streamflow forecasts. 19, 1–15, doi: 10.5194/hess-19-  
551 1-2015.

552 Lu, S., Tong, C.F., Lee, D., Zheng, J.H., Shen, J., Zhang, W., & Yan, Y.X. (2015). Propagation of  
553 tidal waves up in Yangtze Estuary during the dry season. *J. Geophys. Res. Ocean.*, 120,  
554 6445-6473, doi:10.1002/2014JC010414.

555 Mandal, S., Witz, J.A., & Lyons, G.J. (1992). Reduced order ARMA spectral estimation of ocean  
556 waves. *Applied Ocean Research*, 14, 303-312, doi: 10.1016/0141-1187(92)90034-H.

- 557 Matte, P., Jay, D.A., & Zaron, E.D. (2013). Adaptation of Classical Tidal Harmonic Analysis to  
558 Nonstationary Tides, with Application to River Tides. *J. Atmos. Ocean. Technol.*, 30, 569-  
559 589, doi:10.1175/JTECH-D-12-00016.1.
- 560 Matte, P., Secretan, Y., & Morin, J. (2014). Temporal and spatial variability of tidal-fluvial  
561 dynamics in the St. Lawrence fluvial estuary: An application of nonstationary tidal  
562 harmonic analysis. *J. Geophys. Res. Oceans*, 119, 5724-5744, doi:10.1002/2014JC009791.
- 563 Minguez, R., Abascal, A.J., Castanedo, S., & Medina, R. (2012). Stochastic Lagrangian  
564 trajectory model for drifting objects in the ocean. *Stoch Environ Res Risk Assess*, 26:1081-  
565 1093, doi: 10.1007/s00477-011-0548-7.
- 566 Mirzavand, M. & Ghazavi, R. (2015). A stochastic modelling technique for groundwater level  
567 forecasting in an arid environment using time series methods. *Water Resources*  
568 *Management*, 29, 1315-1328, doi:10.1007/s11269-014-0875-9.
- 569 Pan, H.D., Guo, Z., Wang, Y.Y., & Lv, X.Q. (2018). Application of the EMD method to river  
570 tides. *J. Atmos. Ocean. Technol.*, 35, 809–819, doi:10.1175/JTECH-D-17-0185.1.
- 571 Pawlowicz, R., Beardsley, B., & Lentz, S. (2002). Classical tidal harmonic analysis including  
572 error estimates in MATLAB using T\_TIDE. *Comput. Geosci.*, 28, 929-937,  
573 doi:10.1016/S0098-3004(02)00013-4.
- 574 Petaccia, P., Serravall, R., & Pellicano, F. (2006). Improved method of sea level forecasting at  
575 Venice (Northern Adriatic Sea). *Communications in Nonlinear Science and Numerical*  
576 *Simulation*, 11, 281-296, doi: 10.1016/j.cnsns.2004.11.008.
- 577 Peters, T.C., Kar, T.R., Jamas, P.F., Knight, R., & Easterlin, D. (1998). First difference method:  
578 Maximizing station density for the calculation of long-term global temperature change. *J.*



579        *Geophys. Res. Atmospheres.*, 103, 967-974, doi: 10.1029/98JD01168.

580    Savenije, H.H.G. (2015). Prediction in ungauged estuaries: An integrated theory. *Water Resour.*  
581        *Res.*, 51, 2464-2476, doi:10.1002/2015WR016936.

582    Shibata, R. (1976). Selection of the order of an autoregressive model by Akaike's information  
583        criterion. *Biometrika*, 63, 117-126, doi: 10.2307/2335091.

584    Torres, J.L., García, A., Blas, M. D., & Francisco, A. D. (2005). Forecast of hourly average wind  
585        speed with ARMA models in Navarre (Spain). *Solar Energy*, 79, 65–77, doi:  
586        10.1016/j.solener.2004.09.013.

587    Turki, I., Laignel, B., Kakeh, N., Chevalier, L., & Costa, S. (2015). A new hybrid model for  
588        filling gaps and forecast in sea level: application to the eastern English Channel and the  
589        North Atlantic Sea (western France). *Ocean Dynamics*, 65(4), 509-521, doi:  
590        10.1007/s10236-015-0824-z.

591    Zhang, E. F., Savenije, H. H. G., Chen, S.L., & Mao, X.H. (2012). An analytical solution for tidal  
592        dynamics in the Yangtze Estuary, China. *Hydrol. Earth Syst. Sci. Discuss.*, 9, 2213–2244,  
593        doi: 10.5194/hessd-9-2213-2012.